Homogenization of elastic–viscoplastic composites by the Mixed TFA

Homogenization of elastic-viscoplastic composites by the Mixed TFA

F. Covezzi[1] - S. de Miranda[1] - S. Marfia[2] - E. Sacco[2*]

February 2, 2017

[1]DICAM, University of Bologna, Bologna, Italy

[2]DICeM, University of Cassino and Southern Lazio, Cassino, Italy

Abstract

A new homogenization technique, based on the Transformation Field Analysis, able to determine the overall behavior of viscoplastic heterogeneous materials, is proposed. This method is derived developing a variational formulation of the compatibility and evolution equations governing two classical elastic-viscoplastic models, i.e. Perzyna and Perić models. A representation form for the stress field and the plastic multiplier is defined on the representative volume element (RVE) of the composite material, resulting in a significant reduction of the history variables ruling the evolution problem. A numerical procedure is developed integrating the evolution equation by a backward-Euler algorithm and solving the single time step developing a specific form of the predictor corrector technique. The accuracy of the proposed homogenization method is assessed through some numerical examples for elastic-viscoplastic composites. The applications aim to verify the effectiveness of the presented technique in modeling the elastic-viscoplastic composite behavior adopting a reduced number of history variables. The homogenization results are compared with the ones obtained by nonlinear finite element micromechanical analyses.

Keywords: Homogenization; Elastic-viscoplastic material; Variational formulation; TFA.

1 Introduction

The use of composite materials has become of paramount importance in different fields of engineering due to their high performance properties such as light weight and high resistance. The mechanical response of structural elements made of composite materials is significantly influenced by the heterogeneous microstructure of the material and by the nonlinear phenomena occurring in the constituents.

*Corresponding author: Elio Sacco (sacco@unicas.it)

Composites are characterized by different types of nonlinearity depending of the nature of the constituents; in fact, they can be subjected to damage, fracture, plastic and viscous phenomena that have to be properly modeled in order to reproduce the mechanical behavior of the material. In particular, composites with metal [1] or polymer [19] matrices present significant viscoplastic effects that cannot be neglected in designing structural elements made of these materials.

In order to properly model the behavior of composite structures, multiscale techniques can be adopted; when the problem is solved using nonlinear finite element analyses (FEA) both at the material and at the structural level, i.e. the FE^2 multiscale scheme is adopted, the large number of history variables can induce high computational burden resulting in excessive computing time. In order to obtain an efficient numerical tool, reducing the number of history variables, analytical or approximated nonlinear homogenization techniques can be adopted to derive the nonlinear overall response of the composite materials. Concerning the homogenization problem of viscoplastic composites, several techniques have been adopted in literature. Among the others, very recently, Czarnota et al. [7] presented a homogenization technique based on an additive tangent Mori–Tanaka scheme in order to study two-phase composites characterized by phases with nonlinear elastic–viscoplastic behavior and spherical inclusions. Mareau and Berbenni [22] presented a homogenization technique for heterogeneous elastic-viscoplastic materials based on the self-consistent approximation. Agoras et al. [2] presented an alternative technique of the incremental variational procedure of Lahellec and Suquet [21] considering a time-incremental variational formulation for the strain-rate potential of the elastic-viscoplastic composite and defining a homogenization problem with nonuniform "eigenstrain rates" in the phases. They adopted the variational procedure proposed in [29] to handle the nonlinearity and the heterogeneity of the properties in the phases.

An effective approach for reducing the history variables is the Transformation Field Analysis (TFA), originally proposed by Dvorak [10]. The TFA approach is able to determine the behavior of the representative volume element (RVE) of the composite material taking into account the nonlinear phenomena occurring in the constituents by means of the presence of an inelastic strain field.

Lately, the TFA scheme has been adopted to study the response of several nonlinear composites considering a uniform, piece-wise uniform or nonuniform distribution of the inelastic strain and different procedures to evaluate the evolution of the history variables. In particular, the TFA piece-wise uniform approach has been proposed in [11] for evaluating the response of inelastic composites, with elastic-plastic, viscoplastic, or viscoelastic phases. A piece-wise uniform procedure has been adopted in [5] to study the effects of viscoplasticity and damage in metal matrix composites and in [31] to model the nonlinear response of masonry material. A refined procedure, nonuniform TFA (NTFA), considering a nonuniform distribution of the inelastic strain in the material, has been proposed in [25, 26]. They modeled the inelastic strain as a linear combination of modes, evaluated by nonlinear pre-analyses. The evolutive problem has been solved in terms of reduced variables. The NTFA approach has been adopted to model different composite materials, e.g. it has been used to study the polycrystal plasticity in [12, 13], the elastic-viscoplastic response of composite materials in [30], the three dimensional behavior of metal matrix composites in [14, 15] and the response of elastoplastic porous materials in [20]. An improvement of the evolutive formulation in the framework of NTFA has been presented in [17, 16]

proposing the pRBMOR procedure. A piece-wise nonuniform NUTFA approach has been proposed in [23, 33], considering the inelastic strain as a linear combination of analytical inelastic modes with the history variables evaluated on the basis of the continuum evolutive equations. The procedure has been recently adopted to study the behavior of porous SMA [32]; an extension of the NUTFA to the case of composites subjected to cohesive fractures has been proposed in [24]. The main differences between the approaches presented in [17, 16] and in [33] have been described in [18].

Although many efforts have been done in order to improve the nonuniform TFA approach, two key aspects of TFA are still object of research: they concern the approximation of the inelastic field and the solution of the evolution problem that are directly related to the number of history variables.

In this context, the aim of this paper is to propose a new nonuniform TFA approach to model the mechanical response of composites characterized by elastic-viscoplastic constitutive law of the constituents. In particular, two slightly different elastic-viscoplastic models, available in literature (Perzyna and Perić models [28, 27]), are considered for the constituents.

The presented homogenization procedure is based on the technique proposed in [6], limited to the case of elastoplastic phenomena, and herein extended to viscoplasticity. The response of the composite material is studied dividing its RVE in subdomains. The main idea is to approximate the inelastic strain on the basis of a representation of the stress field and of the plastic multiplier on each subdomain of the RVE, by means of the equations ruling the constitutive laws. This choice is motivated by the fact that the stress field becomes the primary variable so that its accuracy can be directly prescribed by assigning a proper approximation; moreover, as the inelastic strain is derived by the stress parameters, the number of variables is reduced. An innovative procedure to solve the evolution equations involving the viscoplastic strain is proposed; the evolution laws are formulated by means of the complementary approach leading to new variational equations; this aspect represents the main difference of the proposed approach with respect to the one discussed in [6]. It could be remarked that the use of the complementary approach for the evolutive law can reduce the classical stiffening effect of the homogenized material, occurring when TFA-based techniques are adopted.

Numerical results are presented to assess the effectiveness of the proposed TFA approach comparing the homogenization results with the mechanical response obtained adopting nonlinear finite element micromechanical analyses. Moreover, a numerical study of a composite, subjected to complex loading histories, is performed remarking the capability of the procedure in reproducing the nonlinear mechanical response of the viscoplastic composite material.

In Section 2 the homogenization of the nonlinear composite together with the constitutive viscoplastic models are presented; in Section 3 the TFA approach is detailed for viscoplastic composites; in Section 4 the numerical procedure is illustrated; numerical applications are reported in Section 5 and conclusion remarks are given in Section 6.

2 Homogenization for nonlinear composite

This section is focused on the elastic-viscoplastic homogenization problem for composite materials. The problem is formulated in the framework of small strains and displacements assumption, considering the plane stress condition. The standard matrix (Voigt) notation is adopted and, hence, the stress, the total strain and the inelastic strain tensors are represented as 3-component vectors, $\boldsymbol{\sigma}$, $\boldsymbol{\varepsilon}$ and $\boldsymbol{\pi}$, respectively. In general, the fourth-order tensors are represented as matrices and, in particular, the fourth-order constitutive tensor is represented as a 3×3 matrix $\mathbf{C}$. Moreover, the adjoint compatibility and equilibrium operators are represented as 3×2 and 2×3 differential matrices $\mathbf{D}$ and $\mathbf{D}^T$, respectively.

First, the constitutive model describing the elastic-viscoplastic behavior of the constituents is introduced and, then, the homogenization problem is presented.

2.1 Elastic-viscoplastic constitutive model

Viscoplasticity indicates a model where both rheologic and plastic effects are taken into account in order to describe the behavior of the material. In particular, a time dependence of the stress and strain state is introduced due to the viscous properties of the medium, while the plastic properties depend on the loading path. As a result, the model becomes both time and loading history dependent.

According to Perzyna [28], there are two different classes of viscoplastic materials: elasto-viscoplastic materials and elastic-viscoplastic materials. The former are the class of materials that show viscous properties in both elastic and plastic regions, while the latter exhibit viscous properties in the plastic region only. Here, this second class will be considered. The elastic-viscoplastic constitutive model is formulated assuming the existence of a dissipation potential and of an elastic domain, in which there are no viscous effects.

Based on the assumption that the viscous properties manifest themselves only once the plastic state is reached, the strain rate can be split into an elastic and inelastic part, where the latter represents combined viscous and plastic effects. In addition, since the material does not show viscous properties in the elastic region, the classical Mises yield function is considered in the framework of associated plasticity [9]. In particular, the elastic perfectly plastic material is considered.

The assumption of perfect plastic material is introduced only to get an easier formulation, but kinematic and/or isotropic hardening effects can be introduced in the procedure, without any particular problem. Hence, the assumption of perfect plasticity is not strictly necessary for the proposed procedure. The initial yield condition (or static yield condition) is:

$$f(\boldsymbol{\sigma}) = q - \sigma_y \qquad \text{with} \quad q = \sqrt{\frac{3}{2}\,\boldsymbol{\sigma}^T \mathbf{M}\,\boldsymbol{\sigma}}\,, \tag{1}$$

where σ_y is the yield stress and

$$\mathbf{M} = \frac{1}{3}\begin{bmatrix} 2 & -1 & 0 \\ -1 & 2 & 0 \\ 0 & 0 & 6 \end{bmatrix}.$$

Introducing a dissipation potential $\Phi^*(\boldsymbol{\sigma})$, the flow rule is given by deriving the potential $\Phi^*(\boldsymbol{\sigma})$ with respect to the stress state:

$$\dot{\boldsymbol{\pi}} = \frac{\partial \Phi^*(\boldsymbol{\sigma})}{\partial \boldsymbol{\sigma}}. \tag{2}$$

Two different types of dissipation potentials are herein considered, that can be found in the literature:

- the potential proposed by Perzyna [28]:

$$\Phi^*(\boldsymbol{\sigma}) = \begin{cases} \frac{\sigma_y}{\mu}\left[\frac{1}{1+\epsilon} + \frac{\epsilon}{1+\epsilon}\Theta(\boldsymbol{\sigma})^{\frac{1+\epsilon}{\epsilon}}\right] & \text{if } f(\boldsymbol{\sigma}) \geq 0 \\ 0 & \text{if } f(\boldsymbol{\sigma}) < 0 \end{cases}, \tag{3}$$

  with $\Theta(\boldsymbol{\sigma}) = q/\sigma_y - 1$,

- the potential proposed by Perić [27]:

$$\Phi^*(\boldsymbol{\sigma}) = \begin{cases} \frac{\sigma_y}{\mu}\left[\frac{1}{1+\epsilon} + \frac{\epsilon}{1+\epsilon}\Theta(\boldsymbol{\sigma})^{\frac{1+\epsilon}{\epsilon}} - \Theta(\boldsymbol{\sigma})\right] & \text{if } f(\boldsymbol{\sigma}) \geq 0 \\ 0 & \text{if } f(\boldsymbol{\sigma}) < 0 \end{cases}, \tag{4}$$

  with $\Theta(\boldsymbol{\sigma}) = q/\sigma_y$.

In equations (3) and (4), μ is a viscosity-related parameter, ϵ is the dimensionless rate sensitivity parameter, with $\epsilon \in (0,1)$ and $\Theta(\boldsymbol{\sigma})$ a function that depends on the yield surface.

The inelastic strain, therefore, becomes:

$$\dot{\boldsymbol{\pi}} = \dot{\xi}\,\mathbf{N} \qquad \text{with } \mathbf{N} = \frac{\partial f}{\partial \boldsymbol{\sigma}} = \frac{\partial q}{\partial \boldsymbol{\sigma}}, \tag{5}$$

where ξ ($\dot{\xi} \geq 0$) is the plastic multiplier.

Differentiating the dissipation potential, it results:

- for the Perzyna model from equation (3):

$$\dot{\xi} = \begin{cases} \frac{1}{\mu}\left[\left(\frac{q}{\sigma_y} - 1\right)^{1/\epsilon}\right] & \text{if } f(\boldsymbol{\sigma}) \geq 0 \\ 0 & \text{if } f(\boldsymbol{\sigma}) < 0 \end{cases}, \tag{6}$$

or, equivalently:

$$\dot{\xi} = \frac{1}{\mu}\left(\left\langle \frac{q}{\sigma_y} - 1 \right\rangle_+\right)^{1/\epsilon}, \tag{7}$$

- for the Perić model from equation (4):

$$\dot{\xi} = \begin{cases} \dfrac{1}{\mu}\left[\left(\dfrac{q}{\sigma_y}\right)^{1/\epsilon} - 1\right] & \text{if } f(\boldsymbol{\sigma}) \geq 0 \\ 0 & \text{if } f(\boldsymbol{\sigma}) < 0 \end{cases}, \tag{8}$$

or, equivalently:

$$\dot{\xi} = \frac{1}{\mu}\left\langle \left(\frac{q}{\sigma_y}\right)^{1/\epsilon} - 1 \right\rangle_+ . \tag{9}$$

As consequence of equation (1), the normal vector defined in formula (5) results:

$$\mathbf{N}(\boldsymbol{\sigma}) = \frac{3}{2\,q}\,\mathbf{M}\,\boldsymbol{\sigma}\,. \tag{10}$$

It can be remarked that the classical Kuhn-Tucker loading-unloading conditions do not govern the problem in case of rate dependent plasticity. In fact, when plasticity is reached, the updated stress state generally lies outside the yield surface, i.e. $f(\boldsymbol{\sigma}) > 0$. This is in contrast with the rate independent case, where the condition $f(\boldsymbol{\sigma}) = 0$ forces the updated stress state to lie on the yield surface when there is a plastic flow [9].

The crucial difference between the elastoplastic and the elastic-viscoplastic model relies on the definition of the flow rule which describes the evolution of the inelastic field. In fact, for elastic-viscoplastic materials, equation (5) is actually time-dependent, i.e. the time scale of the problem affects the evolution of $\boldsymbol{\pi}$. In addition, the plastic multiplier is not an independent variable of the problem, but it is an explicit function of the stress state and of the flow stress σ_y .

Finally, introducing the modified plastic multiplier as:

$$\dot{\gamma} = \frac{1}{2\,q}\dot{\xi}\,, \tag{11}$$

the flow rule equation (5) can be rewritten in the equivalent form:

$$\dot{\boldsymbol{\pi}} = \dot{\gamma}\,3\,\mathbf{M}\,\boldsymbol{\sigma}\,. \tag{12}$$

Note that the modified plastic multiplier $\dot{\gamma}$ has not a clear physical meaning, but it is introduced with the only aim to simplify the form of the evolution equation for the following developments. In fact, in case of hardening, the accumulated plastic strain should be evaluated from the plastic multiplier $\dot{\xi}$ and not from the modified plastic multiplier $\dot{\gamma}$.

2.2 Homogenization problem

Let a composite material be considered with a RVE, whose domain is denoted as Ω. It is assumed that some constituents of the composite present a nonlinear response, and that it is not characterized by either cracks and voids or sliding and decohesion.

In the following, the micromechanical and homogenization problem is formulated in terms of the prescribed average strain $\bar{\boldsymbol{\varepsilon}}$ in Ω, so that the displacement and strain fields are represented in the domain Ω, respectively, as:

$$\mathbf{u} = \bar{\mathbf{u}} + \widetilde{\mathbf{u}} \tag{13}$$

$$\boldsymbol{\varepsilon} = \bar{\boldsymbol{\varepsilon}} + \widetilde{\boldsymbol{\varepsilon}} \tag{14}$$

where $\bar{\mathbf{u}}$ is the vector of the displacement field associated to the homogenized material subjected to the prescribed average strain vector $\bar{\boldsymbol{\varepsilon}}$, while $\widetilde{\mathbf{u}}$ is the perturbation of the displacement field due to the presence of the heterogeneities and $\widetilde{\boldsymbol{\varepsilon}}$ is its associated perturbation strain vector, i.e. $\widetilde{\boldsymbol{\varepsilon}} = \mathbf{D}\widetilde{\mathbf{u}}$. The homogenization problem consists in finding the displacement field $\widetilde{\mathbf{u}}$, the strain field $\widetilde{\boldsymbol{\varepsilon}}$, the inelastic strain field $\boldsymbol{\pi}$, the stress field $\boldsymbol{\sigma}$, which satisfy the compatibility, the constitutive and the equilibrium with zero body forces equations:

$$\widetilde{\boldsymbol{\varepsilon}} = \mathbf{D}\widetilde{\mathbf{u}} \tag{15}$$

$$\boldsymbol{\sigma} = \mathbf{C}\left(\boldsymbol{\varepsilon} - \boldsymbol{\pi}\right) \tag{16}$$

$$\mathbf{0} \qquad \mathbf{D}^T\boldsymbol{\sigma} \tag{17}$$

together with the evolution equations described in the previous section. Proper boundary conditions, which will be specified in the following, complete the problem. The perturbation strain $\widetilde{\boldsymbol{\varepsilon}}$ has to be characterized by null average, so that:

$$\frac{1}{V}\int_\Omega \widetilde{\boldsymbol{\varepsilon}}\; dV = \mathbf{0} \qquad \Rightarrow \qquad \frac{1}{V}\int_\Omega \boldsymbol{\varepsilon}\, dV = \bar{\boldsymbol{\varepsilon}}\,, \tag{18}$$

where V is the volume of Ω.

Note that the representation form for the strain, reported in formula (14), appears very suitable and it is commonly adopted, mainly for periodic materials, as the null average condition for the perturbation strain can be almost easily prescribed by introducing suitable boundary conditions on the displacement field. As a consequence of this choice, the formulation of the problem is written in terms of perturbation strain. Of course, the total strain can be easily computed adding the average strain to the perturbation one at each point of the domain.

Finally, the average stress $\bar{\boldsymbol{\sigma}}$ is defined as:

$$\bar{\boldsymbol{\sigma}} = \frac{1}{V}\int_\Omega \boldsymbol{\sigma}\, dV\,. \tag{19}$$

3 Computational homogenization technique

The nonlinear homogenization problem defined by all the equations reported in the previous section can be solved for a given RVE adopting classical finite element analyses involving a large number of history variables. This approach induces a high computational burden when the homogenization is integrated into a multiscale procedure. In order to reduce the number of history variables, a TFA based technique is proposed, considering a nonuniform inelastic strain distribution in the RVE. This can be performed introducing directly a representation form for the inelastic strain distribution following the classical approach proposed in literature [25, 26, 33, 16]. An alternative and innovative way for representing the inelastic strain field can be achieved recalling equation (12) and properly representing the stress field and the plastic multiplier in the RVE. In particular, motivated by very good results obtained in stress recovery techniques based on the weak enforcement of the compatibility condition [35, 3, 4, 8], here the problem is formulated following a complementary approach. The proposed TFA formulation is named in the following as Mixed Transformation Field Analysis (MxTFA).

The weak forms of the compatibility and of the modified plastic multiplier equations are introduced as:

$$\int_\Omega \delta\boldsymbol{\sigma}^T \mathbf{C}^{-1}\boldsymbol{\sigma}\, dV - \int_\Omega \delta\boldsymbol{\sigma}^T \left(\bar{\boldsymbol{\varepsilon}} + \widetilde{\boldsymbol{\varepsilon}} - \boldsymbol{\pi}\right) dV = 0 \quad \forall\, \delta\boldsymbol{\sigma} :\ \mathbf{D}^T\delta\boldsymbol{\sigma} = \mathbf{0}\,, \tag{20}$$

$$\int_\Omega \delta\gamma \left(\dot{\gamma} - \frac{1}{2\,q}\dot{\xi}\left(\boldsymbol{\sigma}\right)\right) dV = 0\,. \tag{21}$$

with $\dot{\xi}\left(\boldsymbol{\sigma}\right)$ given by equation (7) for Perzyna model and by equation (9) for Perić model.

Then, the RVE is divided into n subdomains (or subsets) Ω^j with $j = 1,..,n$, each of them characterized by a volume V^j, such that:

$$\Omega = \bigcup_{j=1}^{n} \Omega^j\,, \qquad V = \sum_{j=1}^{n} V^j\,. \tag{22}$$

The proposed MxTFA exploits the typical approach of mixed stress finite elements in which piecewise continuous representations for the stress components over the domain are allowed and traction continuity among the subdomains is not required. Thus, in the MxTFA the stresses are approximated independently over each subset of the RVE. In particular, the self-equilibrated stress field $\boldsymbol{\sigma}^j$ in the typical $j-$th subset Ω^j , is approximated as (no sum on j):

$$\boldsymbol{\sigma}^j = \mathbf{P}\,\widehat{\boldsymbol{\sigma}}^j\,, \tag{23}$$

where $\mathbf{P}$ is a $3 \times p$ matrix collecting a set of p self-equilibrated stress modes and $\widehat{\boldsymbol{\sigma}}^j$ the vector of the unknown p stress parameters. In other words, the self-equilibrated stress in the subset is represented as linear combination of chosen self-equilibrated modes, ensuring that $\mathbf{D}^T\mathbf{P}\widehat{\boldsymbol{\sigma}}^j = \mathbf{0}$ in Ω^j. In particular, it is assumed a linear approximation for the stress field in the subset Ω^j; consequently, it results $p = 7$

and

$$\mathbf{P} = \begin{bmatrix} 1 & 0 & 0 & x_2 & 0 & x_1 & 0 \\ 0 & 1 & 0 & 0 & x_1 & 0 & x_2 \\ 0 & 0 & 1 & 0 & 0 & -x_2 & -x_1 \end{bmatrix} . \tag{24}$$

The modified plastic multiplier is approximated in each subset Ω^j independently from the representation of the stress field as:

$$\dot{\gamma}^j = \sum_{i=1}^{\rho} r_i\left(\mathbf{x}\right) \dot{\widehat{\gamma}}_i^j = \mathbf{r}^T \dot{\widehat{\boldsymbol{\gamma}}}^j \,, \tag{25}$$

where $\mathbf{r}$ is a set of ρ modes chosen to approximate the function $\dot{\gamma}$ in Ω^j and $\dot{\widehat{\boldsymbol{\gamma}}}^j$ is the vector containing the corresponding coefficients. A piecewise uniform distribution is considered for the modified plastic multiplier, i.e. $\rho = 1$. In the typical $j-$th subset Ω^j, it results:

$$\dot{\gamma}^j = \begin{cases} \frac{1}{\mu V^j} \int_{\Omega^j} \frac{1}{2\,q^j} \left(\left\langle \frac{q^j}{\sigma_y} - 1 \right\rangle_+ \right)^{1/\epsilon} dV & \text{Perzyna} \\ \frac{1}{\mu V^j} \int_{\Omega^j} \frac{1}{2\,q^j} \left\langle \left(\frac{q^j}{\sigma_y} \right)^{1/\epsilon} - 1 \right\rangle_+ dV & \text{Perić} \end{cases} , \tag{26}$$

with

$$q^j = \sqrt{\frac{3}{2} \left(\widehat{\boldsymbol{\sigma}}^j\right)^T \mathbf{Q} \widehat{\boldsymbol{\sigma}}^j} \,, \tag{27}$$

where $\mathbf{Q} = \mathbf{P}^T \mathbf{M} \mathbf{P}$. In the above equation and in the following, the material properties are intended as those of the current subset.

Taking into account the equation (23), the flow rule equation (12) in the subset Ω^j is rewritten in the form:

$$\dot{\boldsymbol{\pi}}^j = \dot{\gamma}^j \, \mathbf{T} \widehat{\boldsymbol{\sigma}}^j \qquad \text{with} \;\; \mathbf{T} = 3\,\mathbf{M}\,\mathbf{P} \,. \tag{28}$$

Equation (28) links the approximation introduced for the stress field in the subset Ω^j, through the flow rule condition, to the one of the inelastic strain rate in that subset.

The total strain at the typical point $\mathbf{x}$ of Ω^j depends on the average strain $\bar{\boldsymbol{\varepsilon}}$ and on the distribution of the inelastic strain $\boldsymbol{\pi}$ in the whole RVE. As a consequence, the perturbation strain field $\widetilde{\boldsymbol{\varepsilon}}^j$ can be split in two contributions:

$$\widetilde{\boldsymbol{\varepsilon}}^j = \widetilde{\boldsymbol{\varepsilon}}^{\varepsilon,j} + \widetilde{\boldsymbol{\varepsilon}}^{\pi,j} = \mathbf{L}^{\bar{\varepsilon},j} \bar{\boldsymbol{\varepsilon}} + \sum_{i=1}^{n} \mathbf{L}^{\pi^i,j} \boldsymbol{\pi}^i \,, \tag{29}$$

where $\widetilde{\boldsymbol{\varepsilon}}^{\varepsilon,j}$ and $\widetilde{\boldsymbol{\varepsilon}}^{\pi,j}$ are the perturbation strains due to the average strain and to the presence of the inelastic field, respectively; $\mathbf{L}^{\bar{\varepsilon},j}$ and $\mathbf{L}^{\pi^i,j}$ are 3×3 localization matrices, whose evaluation is performed using the finite element method. In particular, the $k-$th column of the localization matrices $\mathbf{L}^{\bar{\varepsilon},j}(\mathbf{x})$ is evaluated computing the strain at $\mathbf{x} \in \Omega^j$, when the UC is subjected to the $k-$th component of $\bar{\boldsymbol{\varepsilon}}$ equal to 1 and all the others equal to zero; analogously, the $p-$th column of $\mathbf{L}^{\pi^i,j}(\mathbf{x})$ is evaluated computing the strain at $\mathbf{x} \in \Omega^j$ when the sub-domain Ω^i of the UC is subjected to the $p-$th mode

and all the others equal to zero.

In order to ensure consistency between the representations of stress, total and inelastic strain, the following approximation $\check{\varepsilon}^j$ of the perturbation strain $\tilde{\varepsilon}^j$ is introduced in Ω^j:

$$\check{\boldsymbol{\varepsilon}}^j = \mathbf{I}^s \boldsymbol{\Pi}\, \widehat{\boldsymbol{\varepsilon}}^j \,, \tag{30}$$

where:

$$\mathbf{I}^s = \begin{bmatrix} 1 & 0 & 0 \\ 0 & 1 & 0 \\ 0 & 0 & 2 \end{bmatrix}, \qquad \boldsymbol{\Pi} = \begin{bmatrix} 1 & 0 & 0 & x_1 & 0 & 0 & x_2 & 0 & 0 \\ 0 & 1 & 0 & 0 & x_1 & 0 & 0 & x_2 & 0 \\ 0 & 0 & 1 & 0 & 0 & x_1 & 0 & 0 & x_2 \end{bmatrix},$$

and $\widehat{\boldsymbol{\varepsilon}}^j$ is a vector of unknown parameters. As it can be noted, the above assumption involves a linear representation basis for the stress and the total strain fields and it is different from the choice performed in [6].

The vector $\check{\boldsymbol{\varepsilon}}^j$ is evaluated as the projection of $\widetilde{\boldsymbol{\varepsilon}}^j$ obtained by enforcing the weak form condition:

$$0 = \int_{\Omega^j} \left(\delta\check{\boldsymbol{\varepsilon}}^j\right)^T \left(\check{\boldsymbol{\varepsilon}}^j - \widetilde{\boldsymbol{\varepsilon}}^j\right) dV \,, \tag{31}$$

obtaining:

$$\widehat{\boldsymbol{\varepsilon}}^j = \left(\int_{\Omega^j} \boldsymbol{\Pi}^T \mathbf{I}^s \boldsymbol{\Pi}\, dV\right)^{-1} \int_{\Omega^j} \left(\mathbf{I}^s\boldsymbol{\Pi}\right)^T \widetilde{\boldsymbol{\varepsilon}}^j \, dV \,. \tag{32}$$

Note that Eq. (31) ensures that the average and the first moment of $\check{\boldsymbol{\varepsilon}}^j$ and $\tilde{\boldsymbol{\varepsilon}}^j$ are the same in every subset. This guarantees that the first of Eq. (18) is fulfilled also by $\check{\boldsymbol{\varepsilon}}^j$.

Setting $\widehat{\mathbf{T}} = \int_{\Omega^j} \boldsymbol{\Pi}^T \mathbf{I}^s \boldsymbol{\Pi}\, dV$ and accounting for equation (29), formula (32) becomes:

$$\widehat{\boldsymbol{\varepsilon}}^j = \left(\widehat{\mathbf{T}}^j\right)^{-1} \int_{\Omega^j} \left(\mathbf{I}^s\boldsymbol{\Pi}\right)^T \left(\mathbf{L}^{\varepsilon,j}\bar{\boldsymbol{\varepsilon}} + \sum_{i=1}^{n} \mathbf{L}^{\pi^i,j}\boldsymbol{\pi}^i\right) dV \,. \tag{33}$$

Substituting equations (23), (30), (33) into equations (20) referred to the subset Ω^j, it results:

$$\mathbf{S}^j\, \widehat{\boldsymbol{\sigma}}^j - \left[\left(\bar{\mathbf{P}}^j\right)^T + \mathbf{J}^j\right] \bar{\boldsymbol{\varepsilon}} - \int_{\Omega^j} \left[\mathbf{P}^T \mathbf{I}^s \boldsymbol{\Pi}\, \widehat{\mathbf{T}}^{-1} \int_{\Omega^j} \left(\mathbf{I}^s\, \boldsymbol{\Pi}\right)^T \sum_{i=1}^{n} \mathbf{L}^{\pi^i,j}\boldsymbol{\pi}^i \, dV\right] dV + \int_{\Omega^j} \mathbf{P}^T\boldsymbol{\pi}^j \, dV = \mathbf{0} \,, \tag{34}$$

where it has been set:

$$\begin{aligned} \mathbf{S}^j &= \int_{\Omega^j} \mathbf{P}^T \mathbf{C}^{-1} \mathbf{P}\, dV \,, \\ \bar{\mathbf{P}}^j &= \int_{\Omega^j} \mathbf{P}\, dV \,, \\ \mathbf{J}^j &= \int_{\Omega^j} \left[\mathbf{P}^T \mathbf{I}^s \boldsymbol{\Pi}\, \widehat{\mathbf{T}}^{-1} \int_{\Omega^j} \left(\mathbf{I}^s\, \boldsymbol{\Pi}\right)^T \mathbf{L}^{\varepsilon,j}\, dV\right] dV \,. \end{aligned} \tag{35}$$

The $\mathbf{S}^j$ matrix in Eq. (34) can be interpreted as the inverse of the overall constitutive law for the subset Ω^j on the basis of the introduced stress approximation, so that the term $\mathbf{S}^j\,\widehat{\boldsymbol{\sigma}}^j$ represents an overall elastic strain in Ω^j; the $\mathbf{J}^j$ matrix localizes of the average strain $\bar{\boldsymbol{\varepsilon}}$ in Ω^j, responsible for the total strain in the subset, and the third term depends on the inelastic strain and represents a contribution to the total strain. The last term of Eq. (34) is the overall inelastic strain in the subset Ω^j.

Substituting equations (26) into equation (21) written for the subset Ω^j, it results:

$$0 = \begin{cases} \dot{\gamma}^j - \dfrac{1}{\mu V^j}\displaystyle\int_{\Omega^j} \frac{1}{2q^j}\left(\left\langle \frac{q^j}{\sigma_y} - 1 \right\rangle_+\right)^{1/\epsilon} dV & \text{Perzyna} \\ \dot{\gamma}^j - \dfrac{1}{\mu V^j}\displaystyle\int_{\Omega^j} \frac{1}{2q^j}\left\langle \left(\frac{q^j}{\sigma_y}\right)^{1/\epsilon} - 1 \right\rangle_+ dV & \text{Perić} \end{cases} . \tag{36}$$

Some similarities and differences between the MxTFA formulation, herein presented, and the pRBMOR procedure, proposed in [17, 16], can be highlighted. Concerning the similarities, (a) both techniques require the definition of the inelastic strain fields; (b) pre-analyses are required in order to derive the localization or influence matrices; (c) the matrix $\mathbf{S}^j$ in Eq. (34) finds an equivalent operator in the pRBMOR approach; (d) in both procedures, the evaluation of the history variables is based on a weak formulation of the evolutive equations: in fact, in pRBMOR it is obtained by minimizing an effective potential, while in the MxTFA it is obtained introducing the weak form of the compatibility equation and of the evolution of the plastic multiplier. Regarding the differences, (a) the MxTFA introduces the presence of subdomains; (b) the pRBMOR is based on an approximation of the inelastic strain field, while the MxTFA considers the approximation of the stress field, deriving the inelastic strain from the associated evolutive law; (c) in pRBMOR the modes are directly assigned to the inelastic strain, while in the MxTFA the modes are defined analytically; (d) the pre-analyses for the MxTFA are linear elastic and provide the localization matrices, while in pRBMOR the pre-analyses are nonlinear and they lead to the computation of the inelastic and hardening modes and the localization operators.

Making a comparison between the proposed approach and the NUTFA [33], they both assume that the RVE is subdivided into subsets and that the inelastic strain on each subset is given as a combination of modes. The novelty of the MxTFA relies on the fact that inelastic strain distribution depends on the assumed distribution for the stress and plastic multiplier, that are the independent variables of the problem. In addition, since the weak form of compatibility and plastic admissibility equations are enforced over each subset, the evolutive problem is not solved for every integration point of the domain (as in the NUTFA) but at the subset level, where only the stress and plastic multiplier parameters of each subset are needed to model the material behavior.

4 Numerical procedure

In order to solve the evolution problem, a time-integration technique has to be implemented. In particular, the backward Euler algorithm is adopted; the quantities at previous time t_n are denoted with the subscript n, while the quantities at the current time t have no subscript; the time interval

$t - t_n$ is denoted as $\triangle t$.

At each time step, the solution of the evolution problem is performed by establishing a specific predictor-corrector strategy. A trial state is determined considering the inelastic strain quantities as frozen. In particular a trial value of $q^{j,TR}$ is computed so that a trial plastic multiplier $\triangle\gamma^{j,TR}$ can be evaluated solving the time discretized form of the equation (36). If $\triangle\gamma^{j,TR}$ is equal to zero in all the subsets, the trial state is the solution of the elastic step; otherwise a corrector phase is required. In this case the evolution of modified plastic multiplier in the time step interval occurs, leading to $\triangle\gamma^j > 0$; thus, the inelastic strain field evaluated at the current time step t, is obtained as:

$$\begin{aligned} \boldsymbol{\pi}^j &= \boldsymbol{\pi}_n^j + \triangle\gamma^j \, \mathbf{T} \, \widehat{\boldsymbol{\sigma}}^j \\ &= \mathbf{T} \left(\boldsymbol{\beta}^j + \triangle\gamma^j \widehat{\boldsymbol{\sigma}}^j \right) , \end{aligned} \tag{37}$$

with the components vector $\boldsymbol{\beta}^j$ defined as:

$$\boldsymbol{\beta}^j = \sum_{\tau=0}^{t_n} \triangle\gamma_\tau^j \, \widehat{\boldsymbol{\sigma}}_\tau^j \, , \tag{38}$$

representing the history variables of the problem for subset Ω^j.

The residual form of equations (34) and (36), integrated in the time step, are rewritten as:

$$\mathbf{R}_\sigma^j = \mathbf{S}^j \, \widehat{\boldsymbol{\sigma}}^j - \left[\left(\bar{\mathbf{P}}^j \right)^T + \mathbf{J}^j \right] \bar{\boldsymbol{\varepsilon}} + \widehat{\mathbf{P}}^j \left(\boldsymbol{\beta}^j + \triangle\gamma^j \widehat{\boldsymbol{\sigma}}^j \right) - \sum_{i=1}^{n} \mathbf{K}^{ij} \left(\boldsymbol{\beta}^i + \triangle\gamma^i \widehat{\boldsymbol{\sigma}}^i \right) \tag{39}$$

$$R_\gamma^j = \begin{cases} \triangle\gamma^j - \dfrac{\triangle t}{\mu V^j} \displaystyle\int_{\Omega^j} \frac{1}{2q^j} \left[\left(\frac{q^j}{\sigma_y} - 1 \right)^{1/\epsilon} \right] dV & \text{Perzyna} \\ \triangle\gamma^j - \dfrac{\triangle t}{\mu V^j} \displaystyle\int_{\Omega^j} \frac{1}{2q^j} \left[\left(\frac{q^j}{\sigma_y} \right)^{1/\epsilon} - 1 \right] dV & \text{Perić} \end{cases} \tag{40}$$

with

$$\begin{aligned} \widehat{\mathbf{P}}^j &= \int_{\Omega^j} \mathbf{P}^T \mathbf{T} \, dV \\ \mathbf{K}^{ij} &= \int_{\Omega^j} \left[\mathbf{P}^T \mathbf{I}^s \, \boldsymbol{\Pi} \, \widehat{\mathbf{T}}^{-1} \int_{\Omega^j} \left(\mathbf{I}^s \, \boldsymbol{\Pi} \right)^T \mathbf{L}^{\pi^i, j} \mathbf{T} \, dV \right] dV. \end{aligned} \tag{41}$$

The correction phase consists in solving the nonlinear system of $(7+1)$ n equations (39) and (40) with respect to the unknowns $\widehat{\boldsymbol{\sigma}}^j$ and $\triangle\gamma^j$ defined in each subset, since they are the only information that is stored in order to recover the material state at a given time step. In fact, at the end of each time step, the stress and plastic multiplier parameters allow for the recovery of the stress and inelastic strain field according to Eqs. (23), (37) and (38).

The average stress in the whole UC is then computed according to the equation (45).

The residual and the unknown vectors for each subset are defined as $\mathbf{R}^j = \left\{ \begin{array}{cc} \left(\mathbf{R}_\sigma^j \right)^T & R_\gamma^j \end{array} \right\}^T$ and

$\mathbf{U}^j = \left\{ \begin{array}{cc} \left(\widehat{\boldsymbol{\sigma}}^j\right)^T & \triangle\gamma^j \end{array} \right\}^T$, respectively, so that the full residual and unknown vectors for the whole RVE result $\mathbf{R} = \left\{ \begin{array}{ccccc} \left(\mathbf{R}^1\right)^T & \left(\mathbf{R}^2\right)^T & ... & \left(\mathbf{R}^n\right)^T \end{array} \right\}^T$ and $\mathbf{U} = \left\{ \begin{array}{ccccc} \left(\mathbf{U}^1\right)^T & \left(\mathbf{U}^2\right)^T & ... & \left(\mathbf{U}^n\right)^T \end{array} \right\}^T$. A Newton-Raphson technique is adopted to solve the nonlinear problem $\mathbf{R} = \mathbf{0}$, so that at the typical $[p+1]$ iteration, the following linearized problem has to be solved:

$$\mathbf{R}^{[p]} + \left.\frac{\partial \mathbf{R}}{\partial \mathbf{U}}\right|_{[p]} \delta\mathbf{U} = \mathbf{0}\,, \tag{42}$$

with $\delta\mathbf{U}$ the variation of the whole unknown vector arising between two consecutive iterations. The explicit form of the tangent matrix, whose dimension is $(7+1)\,n \times (7+1)\,n$, takes the following form at the $[p]$-th iteration :

$$\frac{\partial \mathbf{R}}{\partial \mathbf{U}} = \left[\begin{array}{cccc} \frac{\partial \mathbf{R}^1}{\partial \mathbf{U}^1} & \frac{\partial \mathbf{R}^1}{\partial \mathbf{U}^2} & ... & \frac{\partial \mathbf{R}^1}{\partial \mathbf{U}^n} \\ \frac{\partial \mathbf{R}^2}{\partial \mathbf{U}^1} & \frac{\partial \mathbf{R}^2}{\partial \mathbf{U}^2} & ... & \frac{\partial \mathbf{R}^2}{\partial \mathbf{U}^2} \\ & & & \\ ... & ... & ... & ... \\ & & & \\ \frac{\partial \mathbf{R}^n}{\partial \mathbf{U}^1} & \frac{\partial \mathbf{R}^n}{\partial \mathbf{U}^2} & ... & \frac{\partial \mathbf{R}^n}{\partial \mathbf{U}^n} \end{array} \right], \tag{43}$$

where the expression of the generic component is given by:

$$\frac{\partial \mathbf{R}^j}{\partial \mathbf{U}^i} = \left[\begin{array}{cc} \frac{\partial \mathbf{R}_\sigma{}^j}{\partial \widehat{\boldsymbol{\sigma}}^i} & \frac{\partial \mathbf{R}_\sigma{}^j}{\partial \triangle\boldsymbol{\gamma}^i} \\ \frac{\partial R^j_\gamma}{\partial \widehat{\boldsymbol{\sigma}}^i} & \frac{\partial R^j_\gamma}{\partial \triangle\boldsymbol{\gamma}^i} \end{array} \right], \tag{44}$$

with:

$$\begin{aligned}
\frac{\partial \mathbf{R}_\sigma{}^j}{\partial \widehat{\boldsymbol{\sigma}}^i} &= \delta_{ij}\left(\mathbf{S}^j + \widehat{\mathbf{P}}^j \triangle\gamma^j\right) - \mathbf{K}^{ij}\triangle\gamma^i \\
\frac{\partial R^j_\gamma}{\partial \widehat{\boldsymbol{\sigma}}^i} &= \delta_{ij} \begin{cases} \dfrac{\triangle t}{2\mu V^j}\displaystyle\int_{\Omega^j} \frac{1}{q^j}\left\{\frac{1}{q^j}\left(\frac{q^j}{\sigma_y}-1\right)^{1/\epsilon} - \frac{1}{\epsilon\sigma_y}\left(\frac{q^j}{\sigma_y}-1\right)^{1/\epsilon-1}\right\}\frac{\partial q^j}{\partial \widehat{\boldsymbol{\sigma}}^i}dV & \text{Perzyna} \\ \dfrac{\triangle t}{2\mu V^j}\displaystyle\int_{\Omega^j} \frac{1}{q^j}\left\{\frac{1}{q^j}\left[\left(\frac{q^j}{\sigma_y}\right)^{1/\epsilon}-1\right] - \frac{1}{\epsilon\sigma_y}\left(\frac{q^j}{\sigma_y}\right)^{1/\epsilon-1}\right\}\frac{\partial q^j}{\partial \widehat{\boldsymbol{\sigma}}^i}dV & \text{Perić} \end{cases} \\
\frac{\partial \mathbf{R}_\sigma{}^j}{\partial \triangle\boldsymbol{\gamma}^i} &= \delta_{ij}\,\widehat{\mathbf{P}}^j\widehat{\boldsymbol{\sigma}}^j - \mathbf{K}^{ij}\widehat{\boldsymbol{\sigma}}^i \\
\frac{\partial R^j_\gamma}{\partial \triangle\boldsymbol{\gamma}^i} &= \delta_{ij}
\end{aligned}$$

being δ_{ij} Kronecker's delta and

$$\frac{\partial q^j}{\partial \widehat{\boldsymbol{\sigma}}^i} = \frac{3\delta_{ij}}{2} \frac{\mathbf{Q}^j \widehat{\boldsymbol{\sigma}}^j}{\left[\frac{3}{2}\left(\widehat{\boldsymbol{\sigma}}^j\right)^T \mathbf{Q}^j \widehat{\boldsymbol{\sigma}}^j\right]^{\frac{1}{2}}} .$$

Of course, the derivatives are only calculated in the j-th subset if it is actually active. The iterations will stop when the norm of the residual vector, suitably normalized, is lower than a prefixed tolerance.

Once all the unknowns are updated, the average stress in the whole RVE is computed. Thanks to the stress approximation introduced in (23), this can be achieved straightforward as:

$$\bar{\boldsymbol{\sigma}} = \frac{1}{V} \sum_{j=1}^{n} \bar{\mathbf{P}}^j \, \widehat{\boldsymbol{\sigma}}^j \, . \tag{45}$$

Note that the stress distribution could be also evaluated from the constitutive equation involving the total and plastic strain fields. However, as usual in mixed stress approaches, higher accuracy in the stress evaluation can be obtained if it is evaluated directly form the stress parameters.

The algorithm is summarized in Box 1. In addition, a summary of the proposed procedure is shown in Fig. 1.

5 Numerical applications

In this section, the performance of the proposed technique in determining of the overall mechanical behavior of composites is assessed. In particular, composites characterized by a periodic microstructure are considered in the numerical applications, so that a repetitive unit cell (UC) subjected to periodic boundary conditions is studied. It can be pointed out that although many real composites have random microstructures, the study of an equivalent periodic material having a single inclusion and the same phase volume fraction of the random material could give significant information also on the behavior of random composites. Some studies have been proposed in literature on this interesting topic, e.g. [34].

For a rectangular UC of dimensions $2\,a_1 \times 2\,a_2$, considering a Cartesian coordinate system (x_1, x_2) placed at the center of it, the periodic boundary conditions assume the form:

$$\begin{array}{rcll} \widetilde{u}_1\left(a_1, x_2\right) & = & \widetilde{u}_1\left(-a_1, x_2\right) & \forall x_2 \in (-a_2, a_2) \\ \widetilde{u}_2\left(a_1, x_2\right) & = & \widetilde{u}_2\left(-a_1, x_2\right) & \forall x_2 \in (-a_2, a_2) \\ & & & \\ \widetilde{u}_1\left(x_1, a_2\right) & = & \widetilde{u}_1\left(x_1, -a_2\right) & \forall x_1 \in (-a_1, a_1) \\ \widetilde{u}_2\left(x_1, a_2\right) & = & \widetilde{u}_2\left(x_1, -a_2\right) & \forall x_1 \in (-a_1, a_1) \end{array} \quad . \tag{46}$$

The localization matrices $\mathbf{L}^{\bar{\varepsilon},j}$ and $\mathbf{L}^{\pi^i,j}$ employed in the MxTFA are evaluated performing linear elastic finite element analyses of the UC subjected to each component of $\bar{\boldsymbol{\varepsilon}}$ and of $\boldsymbol{\pi}^i$, respectively, determining the perturbation strain at each Gauss point of the finite element mesh. In particular,

Box 1 Integration algorithm for the elastic predictor.

1. Assign a new value of $\bar{\boldsymbol{\varepsilon}}$

2. Given the history variables $\boldsymbol{\beta}^j$ at time t_n, computed by equation (38), evaluate the elastic predictor state in each subset Ω^j from equations (39), (27) and (40)

$$\widehat{\boldsymbol{\sigma}}^{j\,TR} = \mathbf{S}^{j^{-1}} \left\{ \left[\left(\bar{\mathbf{P}}^j \right)^T + \mathbf{J}^j \right] \bar{\boldsymbol{\varepsilon}} + \widehat{\mathbf{P}}^j \boldsymbol{\beta}^j - \sum_{i=1}^{n} \mathbf{K}^{ij} \boldsymbol{\beta}^i \right\}$$

$$q^{j,TR} = \sqrt{\frac{3}{2} \left(\widehat{\boldsymbol{\sigma}}^{j,TR} \right)^T \mathbf{Q}^j \widehat{\boldsymbol{\sigma}}^{j,TR}}$$

$$\triangle\gamma^{j,TR} = \begin{cases} \frac{\triangle t}{\mu V^j} \int_{\Omega^j} \frac{1}{2q^{j,TR}} \left[\left\langle \frac{q^{j,TR}}{\sigma_y} - 1 \right\rangle_+^{1/\epsilon} \right] dV & \text{Perzyna} \\ \frac{\triangle t}{\mu V^j} \int_{\Omega^j} \frac{1}{2q^{j,TR}} \left[\left\langle \frac{q^{j,TR}}{\sigma_y} \right\rangle_+^{1/\epsilon} - 1 \right] dV & \text{Perić} \end{cases}$$

3. Check for admissibility of the trial state at the subset
   if $\triangle\gamma^{j,TR} = 0$ for all the subsets $\Longrightarrow$ the trial state is the solution
   else

   (a) Compute the residuals $\mathbf{R}^{[p]}$ at iteration p from equations (39) and (40)

   (b) if $\left\|\mathbf{R}^{[p]}\right\| > TOL$, where $\left\|\mathbf{R}^{[p]}\right\|$ is the $\mathbf{L}^2$ norm of $\mathbf{R}^{[p]}$

   - compute the tangent $\partial\mathbf{R}/\partial\mathbf{U}$, as defined in (43) to get $\delta\mathbf{U}$ from (42)
   - update $\mathbf{U}^{[p+1]} = \mathbf{U}^{[p]} + \delta\mathbf{U}$, set $p = p + 1$ and go to step 3(a)

   (c) else

   - update the variables

4. Continue

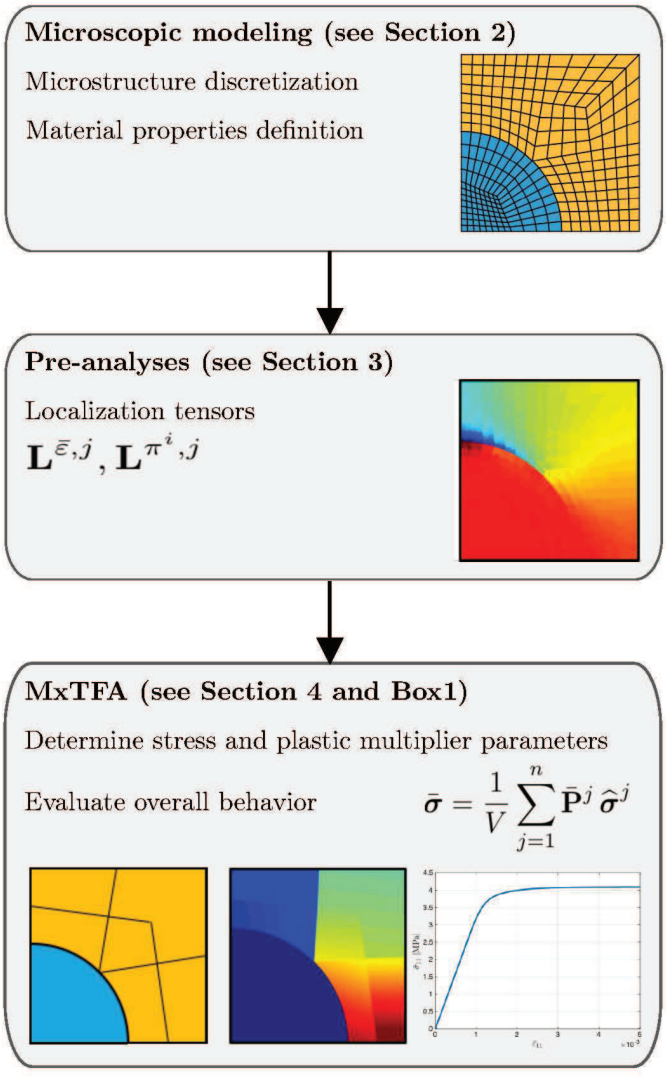

Figure 1: MxTFA: Graphical representation of the procedure.

2D plane stress four-node finite elements are used. The level of refinement of the finite element mesh has been chosen so that the convergence of the FEA solution is ensured. The number of pre-analyses is equal to the 3 components of $\bar{\boldsymbol{\varepsilon}}$ plus the number of the subsets times the 7 components of $\widehat{\boldsymbol{\sigma}}^j$. Furthermore, the matrices defined in (35) are evaluated through numerical integration on the same finite element mesh used for the pre-analyses. Note that the numerical integration could be not strictly necessary in case of simple-shaped subdomains, but when dealing with complex shapes then numerical integration becomes necessary. For sake of uniformity, in this work numerical integration for every matrix is employed.

Two numerical applications are presented: the first is performed on a simple geometry in order to assess the capability of the viscoplastic MxTFA procedure to capture the rate dependency of the problem by applying to the UC an average strain field at increasing strain rates. In order to show the applicability of the proposed technique to different viscoplastic models, both the viscoplastic models introduced by [28] and [27], described above, are adopted.

In the second application, a more realistic geometry is considered and only the viscoplastic model introduced by Perzyna is used, performing analyses for different values the viscosity parameter ϵ at a given strain rate. The ability of the MxTFA technique to reproduce the response of the UC when subjected to loading/unloading strain histories is also investigated.

The results obtained with the proposed homogenization procedure are compared with nonlinear micromechanical analyses, carried out using 2D plane stress four-node quadrilateral finite elements, characterized by elastic and viscoplastic constitutive models. The same finite element meshes adopted for the pre-analyses are used for the nonlinear analyses.

5.1 Test 1 - UC with rectangular inclusion

A periodic heterogeneous material characterized by a viscoplastic matrix and elastic rectangular inclusions is considered. Because of the double symmetry of the UC, only a quarter, whose geometry is represented in Fig. 2, is studied. A unit thickness is assumed and the geometrical parameters are set as follows: $a_1 = 15$ mm, $a_2 = 9$ mm, $b_1 = 5$ mm and $b_2 = 4$ mm, resulting in a volume fraction equal to 15%. The mechanical properties of the constituents are summarized in Table 1, where E, ν, σ_y, μ and ϵ are the Young modulus, the Poisson ratio, the yield stress, the viscosity related parameter and the rate sensitivity parameter, respectively. Both for the elastic pre-analyses and for the nonlinear micromechanical analysis, the quarter of the UC is discretized with a regular mesh composed by 180 finite elements, 150 for the matrix and 30 for the inclusion, as shown in Fig. 3c.

The homogenization analyses are performed considering the subset configurations shown in Fig. 3a and b. In particular, only one subset is used for the elastic inclusion, while the matrix is subdivided into 3 and 5 subsets, resulting, respectively, in $3 \times 7 = 21$ and $5 \times 7 = 35$ history variables of the MxTFA procedure. In fact, for each subset the 7 components of the vector $\boldsymbol{\beta}^j$ represent the history variables of the elastic-viscoplastic problem. In the micromechanical nonlinear finite element analysis, the number of internal variables, considering 4 Gauss points for each finite element and the 3 components of the plastic strain, results $150 \times 4 \times 3 = 1800$, which is significantly higher than the one of the MxTFA.

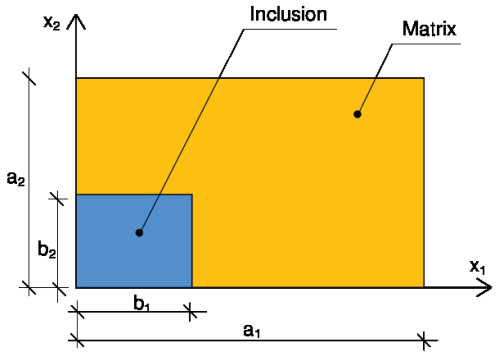

Figure 2: Test 1 - Geometry of the UC for the first numerical application.

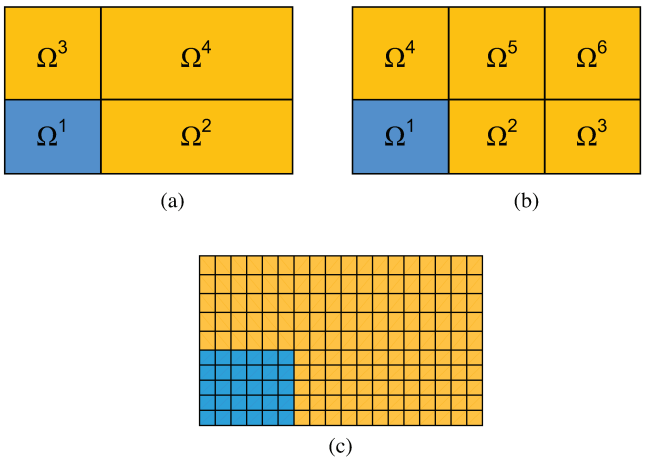

Figure 3: Test 1 - (a) 4 subsets, (b) 6 subsets, (c) Finite element mesh for reference solution and pre-analyses.

Constituent	E [MPa]	ν	σ_y [MPa]	μ [s]	ϵ
Inclusion (elastic material)	25000	0.15	-	-	-
Matrix (viscoplastic material)	2500	0.15	3	500	1 0.1

Table 1: Test 1 - Material properties of the constituents.

The UC is subjected to uni-axial loading along x_1-direction, with an increasing monotone average strain $\bar{\varepsilon}_{11}$ that reaches the maximum value $\bar{\varepsilon}_{11} = 0.005$, prescribing the symmetry boundary conditions. Several simulations are carried out at different strain rates, with two different values of rate sensitivity coefficients.

The mechanical response of the equivalent homogenized material in terms of average stress $\bar{\sigma}_{11}$ versus average strain $\bar{\varepsilon}_{11}$ obtained with the MxTFA compared with the FEA at different strain rates, $\dot{\bar{\varepsilon}}_{11} = 0.05$ s^{-1}, 0.005 s^{-1}, 0.0005 s^{-1}, is shown in Fig. 4 for the 4-subset configuration. In particular, Fig. 4a shows the results for $\epsilon = 1$ using Perić model, while Fig. 4b and 4c for $\epsilon = 0.1$, adopting Perić and Perzyna models, respectively. Results for $\epsilon = 1$ are shown only for the Perić model, since for high value of rate sensitivity parameter the two models lead to similar results. On the contrary, for low values of the rate sensitivity parameter the two models lead to different results, and in particular, it can be seen that for $\epsilon \to 0$ the Perzyna results do not tend to the rate independent curve, but they tend to a curve whose maximum value of the stress is almost twice the one corresponding to the rate independent model. The effectiveness of the MxTFA is determined comparing the results with the FEA ones. In particular, in Table 2 the percentage errors of average stress $\bar{\sigma}_{11}$ at the end of the analyses (i.e. when the average deformation $\bar{\varepsilon}_{11}$ reaches its final value) are collected. In the same table, the elastoplastic results are also shown as the limit case for vanishing strain rate. As it can be noted, there is a very good agreement between the MxTFA predictions and the micromechanical reference solution. The results show that the major influence of the strain rate is observed for the high value of the rate sensitivity parameter ($\epsilon = 1$) reaching a maximum error equal to 2.77% for low value of the strain rate; while only a minor difference can be observed for the low value of the sensitivity parameter ($\epsilon = 0.1$) reaching a maximum error equal to 0.89% for high value of the strain rate. The effect of the strain rate on the response of the material can also be observed: in fact, for a given value of ϵ, higher stress values are obtained at high rates, and the rate independent (i.e. the elastoplastic) solution is approached as the strain rate vanishes. Finally, it can also be remarked that only 4 subsets suffice to achieve very good accuracy in the evaluation of the average stress $\bar{\sigma}_{11}$ at the end of the analysis. The results obtained using the 6-subset partitioning do not provide a substantial improvement in the accuracy and for this reason they are not reported.

Numerical results show also that a linear viscoplastic flow rule ($\epsilon = 1$) could induce a complex inelastic strain distribution, more difficult to be approximated than the one obtained considering a nonlinear viscoplastic flow rule ($\epsilon = 0.1$). In other words, it is not ensured that the inelastic strain distribution coming from a simple (linear) evolution law can be more effectively approximated by the assumed inelastic strain than that coming from a more complex (nonlinear) evolution law.

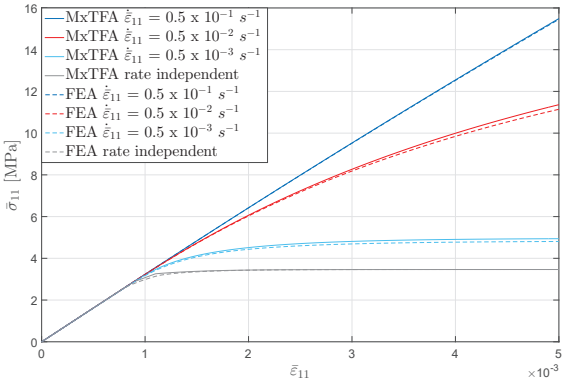

(a)

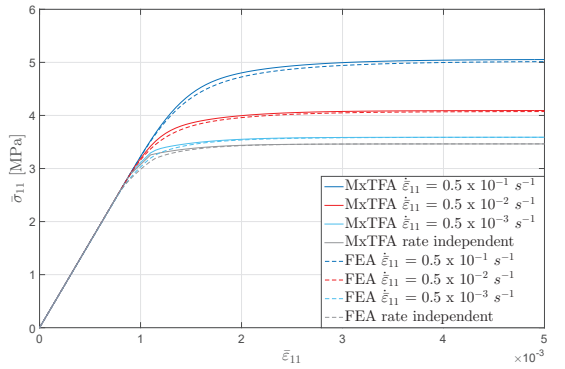

(b)

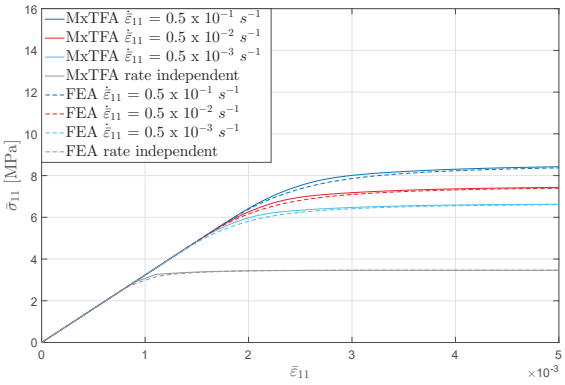

(c)

Figure 4: Test 1 - Mechanical response of the UC subjected to uni-axial loading: (a) $\epsilon = 1$ Perić , (b) $\epsilon = 0.1$ Perić, (c) $\epsilon = 0.1$ Perzyna.

Strain rate $[s^{-1}]$	FEA	MxTFA	Error (%)
$0.5 \cdot 10^{-1}$	15.46	15.49	0.23
$0.5 \cdot 10^{-2}$	11.14	11.36	1.98
$0.5 \cdot 10^{-3}$	4.8	4.94	2.32
rate independent	3.46	3.47	0.02

(a)

Strain rate $[s^{-1}]$	FEA	MxTFA	Error (%)
$0.5 \cdot 10^{-1}$	5.02	5.05	0.78
$0.5 \cdot 10^{-2}$	4.07	4.09	0.47
$0.5 \cdot 10^{-3}$	3.58	3.59	0.04
rate independent	3.46	3.47	0.02

(b)

Strain rate $[s^{-1}]$	FEA	MxTFA	Error (%)
$0.5 \cdot 10^{-1}$	8.37	8.42	0.66
$0.5 \cdot 10^{-2}$	7.40	7.43	0.51
$0.5 \cdot 10^{-3}$	6.61	6.63	0.38
rate independent	3.46	3.47	0.02

(c)

Table 2: Test 1 - Final value of the average stress $\bar{\sigma}_{11}$ [MPa] for uni-axial loading condition; (a) $\epsilon = 1$ Perić model, (b) $\epsilon = 0.1$ Perić model, (c) $\epsilon = 0.1$ Perzyna model.

In addition to the previous results, it might be interesting to inspect the maps of the strain field. In fact, the total strain at the end of the loading history for the two subset configurations are shown in Fig. 5, considering the Perić model, $\epsilon = 0.1$ and strain rate $0.5 \cdot 10^{-2}$ s^{-1}. The total strain $\boldsymbol{\varepsilon}$ is defined, according to Eq. (14), as the sum of two contributions, deriving from the prescribed average strain $\bar{\boldsymbol{\varepsilon}}$ and from the perturbation strain $\widetilde{\boldsymbol{\varepsilon}}$. The latter is defined by Eq. (29) as function of the localization tensors $\mathbf{L}^{\bar{\varepsilon},j}$ and $\mathbf{L}^{\pi^i,j}$, while its approximation $\check{\boldsymbol{\varepsilon}}$ is introduced by Eq. (30). In Fig. 5, two different strain distributions are considered: one coming from the perturbation strain $\widetilde{\boldsymbol{\varepsilon}}$ and the other coming from its approximation $\check{\boldsymbol{\varepsilon}}$. As expected, $\check{\boldsymbol{\varepsilon}}$ determines a smoother distribution of the strain inside the domain with respect to $\widetilde{\boldsymbol{\varepsilon}}$. Moreover, little differences in the local distribution can be observed passing from 4 to 6 subsets.

5.2 Test 2 - UC with a circular inclusion

The UC consists in a circular elastic inclusion embedded in a viscoplastic matrix with volume fraction equal to 25%, as shown in Fig. 6. Thanks to symmetry only one quarter of the UC is modeled applying symmetry boundary conditions. The following geometrical parameters are assumed: $a = 1$ mm and $r = 0.56$ mm. The material parameters are collected in Table 3. From the table it can be observed that the rate sensitivity parameter ϵ is set equal to 0.1, 0.2 or 1.

Fig. 7a shows that for the FEA model employed to perform the linear elastic pre-analyses and to compute the micromechanical reference solution, the quarter of UC has been discretized using 304

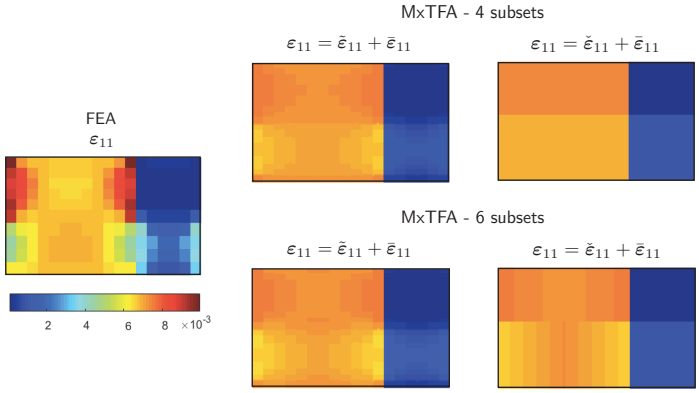

Figure 5: Test 1- Comparison between strain maps coming from FEA and MxTFA.

Constituent	E [GPa]	ν	σ_y [MPa]	μ [s]	ϵ
Inclusion (elastic material)	400	0.20	-	-	-
Matrix (viscoplastic material)	70	0.30	480	500	1 0.2 0.1

Table 3: Test 2 - Material properties for the constituents.

finite elements, 176 for the matrix and 128 for the inclusion: the history variables of the nonlinear micromechanical analysis are equal to $176 \times 4 \times 3 = 2112$. One of the main advantages of the MxTFA approach is that the subsets can have any shape (convex and no-convex shapes): this allows to model complex shapes using a small number of subsets. Anyway, the choice of the subsets is important to reach accurate results, as their shapes can influence the solution. As in finite elements, a suitable choice is to discretize the domain with regular subsets. For this reason, an almost regular discretization in subdomain is performed. In fact, the MxTFA homogenization analyses are performed discretizing the UC with 7 subsets (6 subsets for the matrix and 1 subset for the inclusion), as shown Fig. 7b, resulting in $6 \times 7 = 42$ history variables, significantly lower than the ones of the FEA.

5.2.1 Uni-axial loading along x_2-axis

The UC is subjected to uni-axial loading along the x_2-axis at the constant strain rate $\dot{\bar{\varepsilon}}_{22} = 0.01\text{s}^{-1}$, with the average strain $\bar{\varepsilon}_{22}$ monotonically increased until the final value $\bar{\varepsilon}_{22} = 0.1$. Fig. 8 shows the constitutive response of the equivalent homogenized material in terms of $\bar{\sigma}_{22}$ versus $\bar{\varepsilon}_{22}$ for all the rate sensitivity exponents together with the corresponding FEA reference solution. The rate independent

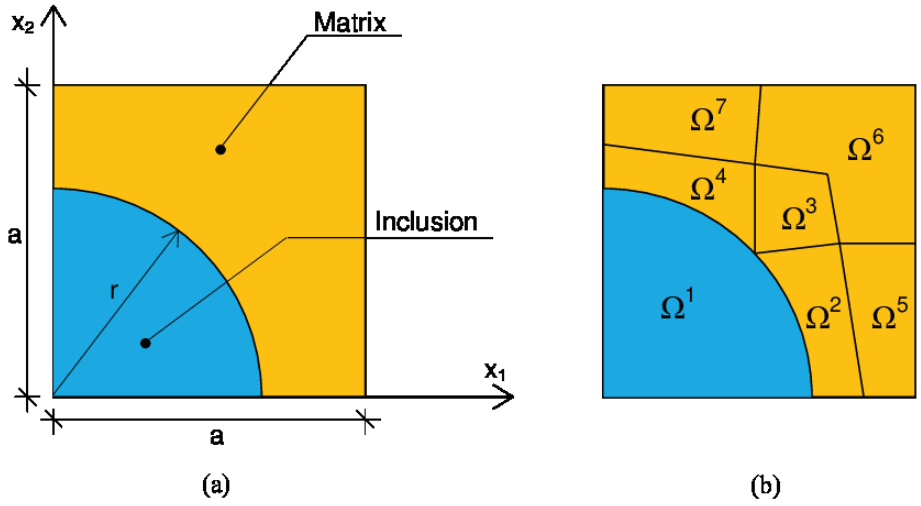

Figure 6: Test 2 - Problem geometry.

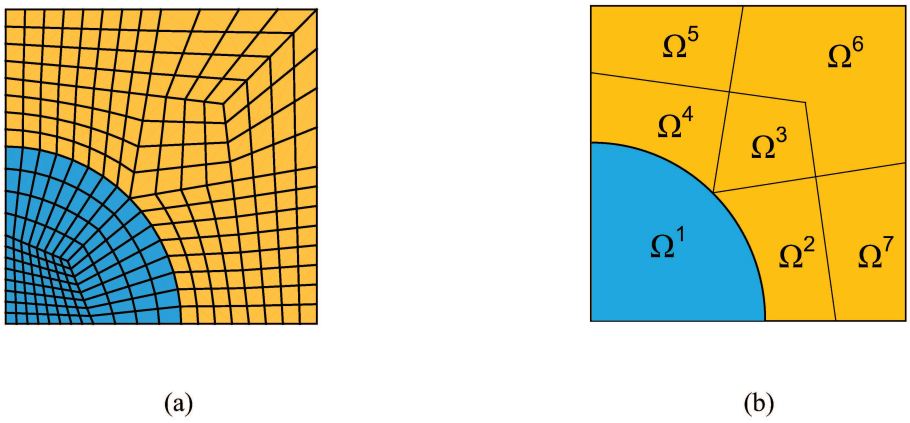

Figure 7: Test 2 - (a) Finite element mesh for reference solution and pre-analyses, (b) Subset discretization.

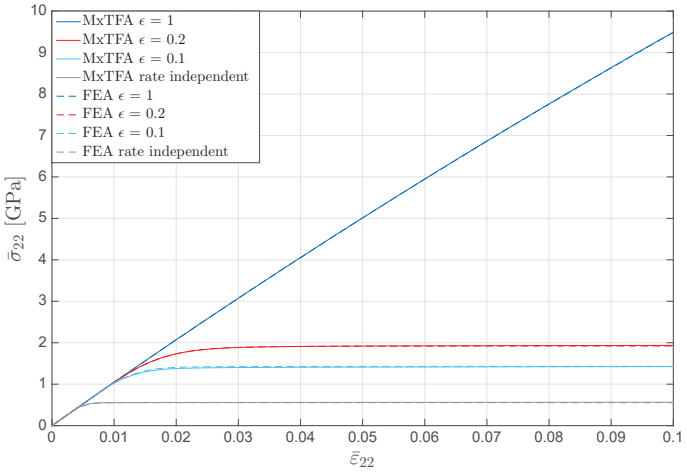

Figure 8: Test 2 - Mechanical response of the UC subjected to uni-axial loading.

ϵ	FEA	MxTFA	Error (%)
1	9.48	9.49	0.06
0.2	1.92	1.94	0.78
0.1	1.43	1.42	0.35
rate independent	0.56	0.57	2.01

Table 4: Test 2 - Final value of the average stress $\bar{\sigma}_{22}$ [GPa] for uni-axial loading condition.

(elastoplastic) solution is also reported, as limit case for $\epsilon \to 0$. The final value of the average stress $\bar{\sigma}_{22}$ obtained with the MxTFA is compared with the reference one deriving from the FEA in Table 4. As expected, different behaviors are observed for different values of ϵ, with higher stress values for higher values of the rate sensitivity parameter. These results highlight that the MxTFA is able to accurately reproduce the overall behavior of the UC also in this case, with the largest error equal to 2.01% for the rate independent case. Moreover, Fig. 9 shows the constitutive behavior of the UC, as well as the behavior of the sole matrix and inclusion, for $\epsilon = 0.2$. In particular, for the UC and each phase the respective average stress versus the respective average strain are reported. Also in this case the very good performance of the MxTFA can be observed.

For the same loading history, the stress and inelastic strain maps for the intermediate rate sensitivity parameter ($\epsilon = 0.2$) at the end of the analysis for the MxTFA and the FEA reference solution are reported in Figs. 10 and 11 respectively, in order to have a better insight of the local distribution of these quantities. A good agreement between the two solutions is observed.

The local error evaluated as the absolute value of the difference between the FEA reference solution and the MxTFA solution is shown in Fig. 12.

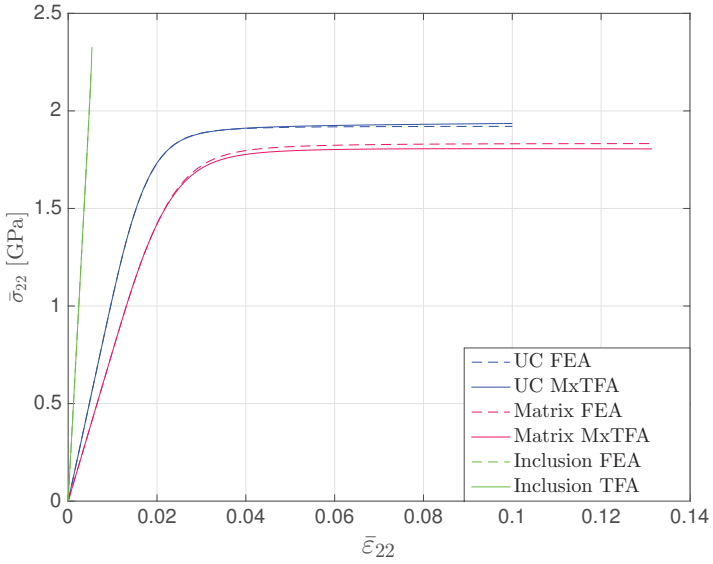

Figure 9: Test 2 - Mechanical response of the UC and the two phases subjected to uni-axial loading ($\epsilon = 0.2$).

5.2.2 Loading/Unloading histories

The UC is considered subjected to the uni-axial loading/unloading history along x_1-axis at a constant strain rate equal to $|\dot{\bar{\varepsilon}}_{11}| = 10^{-2}$ s^{-1}, schematically represented in Fig. 13. The overall response of the UC is reported in Fig. 14 comparing the MxTFA and FEA results for the rate sensitivity parameter equal to $\epsilon = 0.1$ and $\epsilon = 0.2$; also the case of the rate independent elastoplastic solution is reported.

Furthermore, the bi-axial loading/unloading history, shown in Fig. 15, is considered. In Fig. 16a the average stress $\bar{\sigma}_{11}$ is plotted versus the average strain $\bar{\varepsilon}_{11}$ and in Fig. 16b $\bar{\sigma}_{22}$ is plotted versus $\bar{\varepsilon}_{22}$ for MxTFA and FEA considering $\epsilon = 0.1$, $\epsilon = 0.2$ and the rate independent case.

The MxTFA results, obtained for both the uni-axial and bi-axial loading/unloading histories, appear in a very satisfactory agreement with the FEA responses, denoting also in this case the effectiveness of the proposed homogenization procedure.

6 Conclusions

A TFA approach to model the mechanical response of composite materials characterized by viscoplastic phenomena is proposed. It is based on the Transformation Field Analysis and it allows to take into account nonuniform distribution of the inelastic strain in the RVE. Some innovations have been introduced both in the approximation of the inelastic strain field and in the evaluation of the history variables of the problem that lead to an efficient homogenization technique. In particular, the approximation of the inelastic strain field derives from the assumed approximation for the stress and plastic

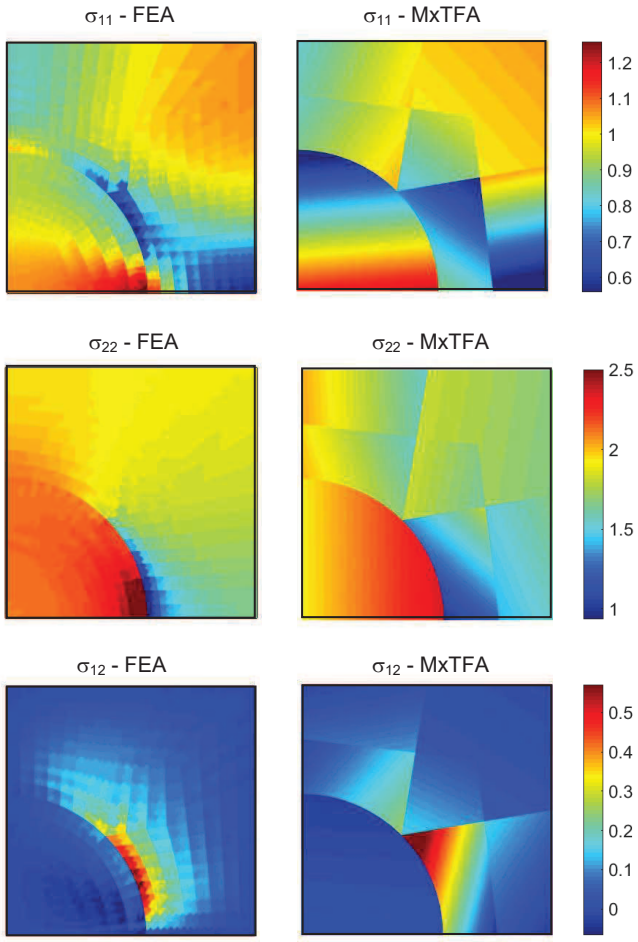

Figure 10: Test 2 - Contour maps of stress [GPa] for $\epsilon = 0.2$.

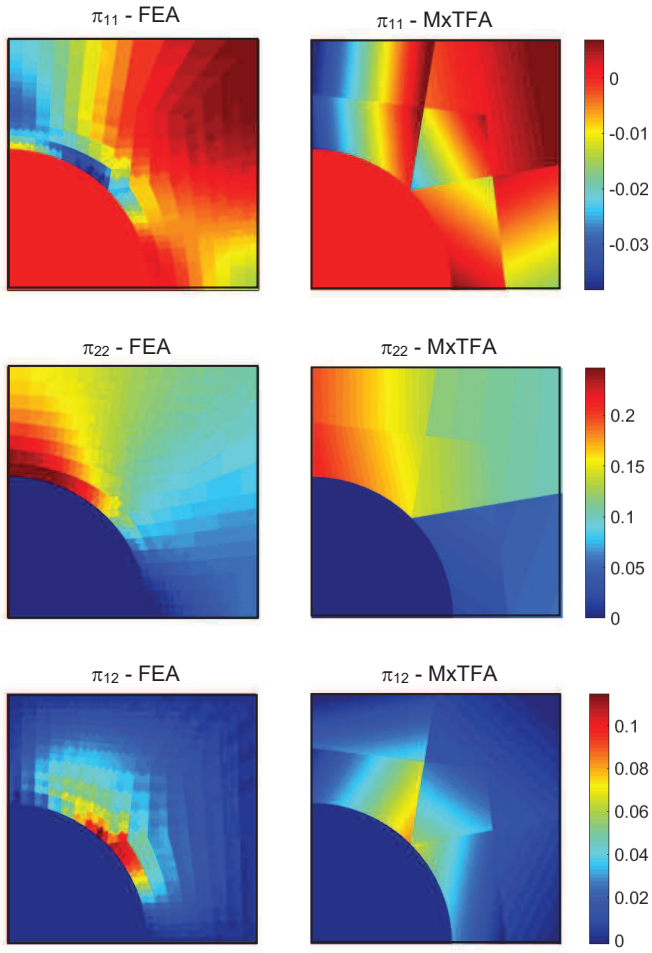

Figure 11: Test 2 - Contour maps of inelastic strain for $\epsilon = 0.2$.

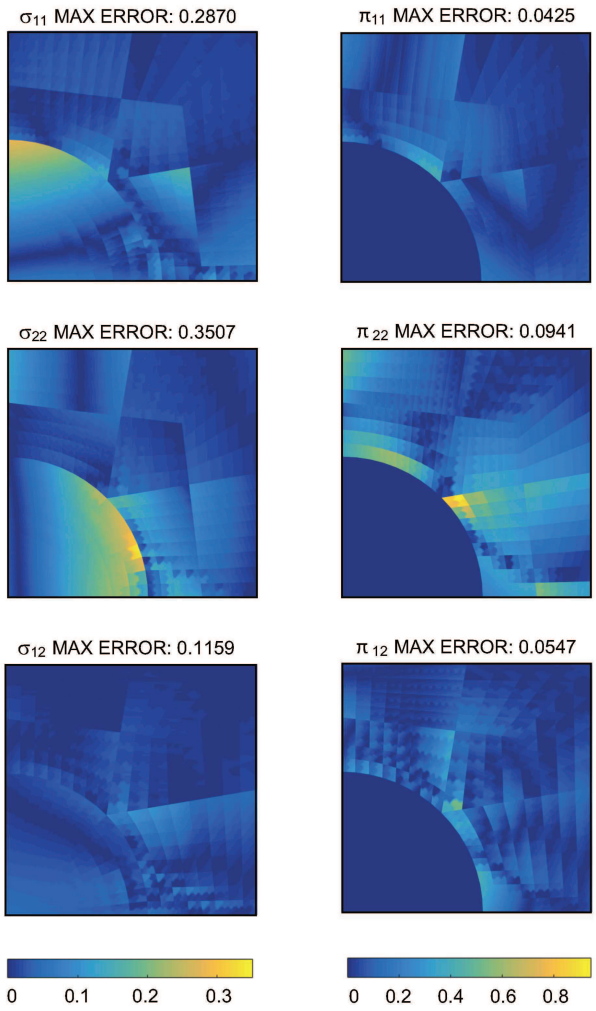

Figure 12: Test 2 - Local error maps of the stress [GPa] and inelastic strain, $\epsilon = 0.2$.

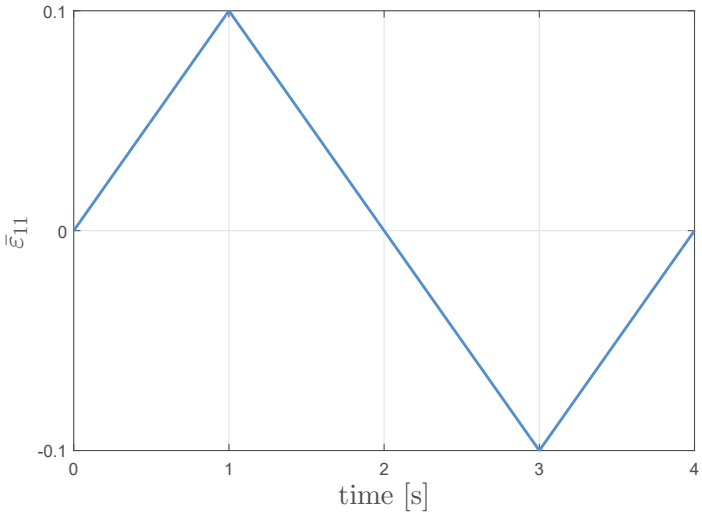

Figure 13: Test 2 - Loading history along x_1-axis.

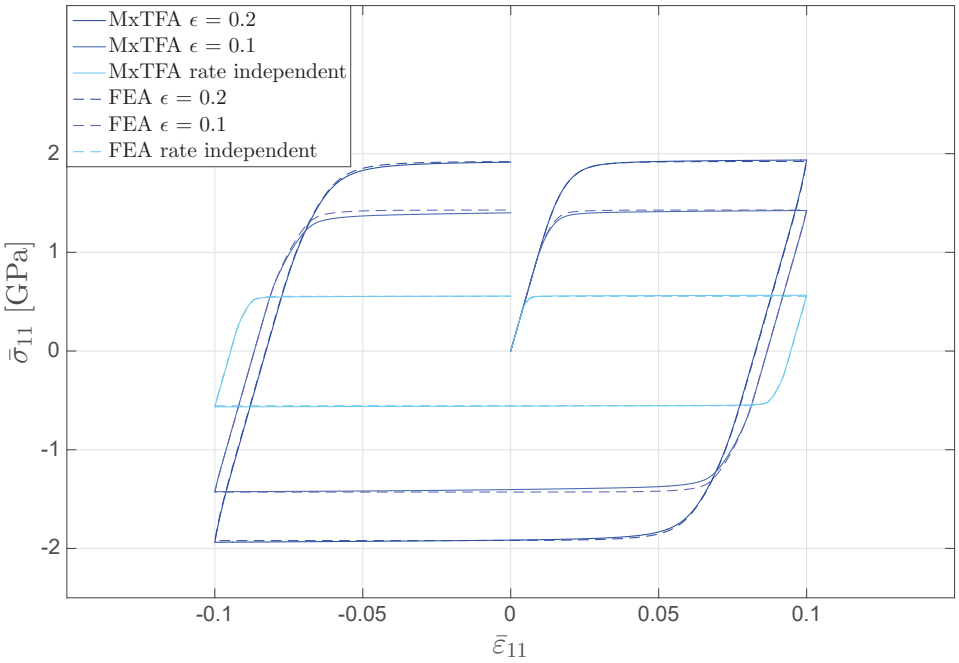

Figure 14: Test 2 - Mechanical response of the UC subjected to a uni-axial loading history.

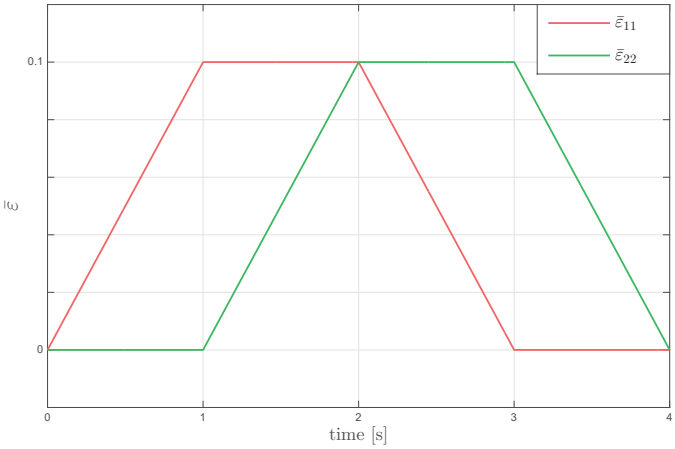

Figure 15: Test 2 - bi-axial loading history.

multiplier, while in other TFA schemes the inelastic modes are directly assigned to this quantity. The evaluation of the history variables is performed at subset level based on the weak formulation of the evolutive problem.

The numerical results show the efficiency of the proposed TFA procedure in reproducing the constitutive overall behavior of periodic composites whose constituents are characterized by elastic-viscoplastic response. In particular, in the first numerical application concerning the analysis of a simple UC subjected to monotonic loading condition the homogenized results are in very good accordance with the mechanical response obtained performing nonlinear finite element micromechanical analyses for all the studied cases. It can be remarked that the MxTFA results are achieved considering only 4 subsets, resulting in a number of history variables more than eighty times lower than in the finite element analyses. The greatest discrepancy in the evaluation of the stress at the end of the loading history (2.77%) is achieved for a higher value of the rate sensitivity parameter and a lower value of the strain rate.

In the second application, a composite with a circular elastic inclusion in a viscoplastic matrix is studied considering both monotonic and loading-unloading uni-axial and bi-axial histories. In this case the number of history variables results fifty times lower than the ones needed in the nonlinear finite element analyses. The Perzyna viscoplastic model is adopted to model the matrix behavior. The MxTFA results show that the homogenization technique is able to reproduce very accurately the FEA results also when the loading histories are very complex. The comparison of the distribution of the stresses and of the inelastic strains on the UC show a very good agreement between MxTFA and FEA also in the evaluation of local quantities.

In case of increasing approximation order for the stress distribution an improvement in the results is surely expected. In the investigated applications, it has been found that the use of higher order approximations leads, generally, to more accurate results with respect to the increase of the number

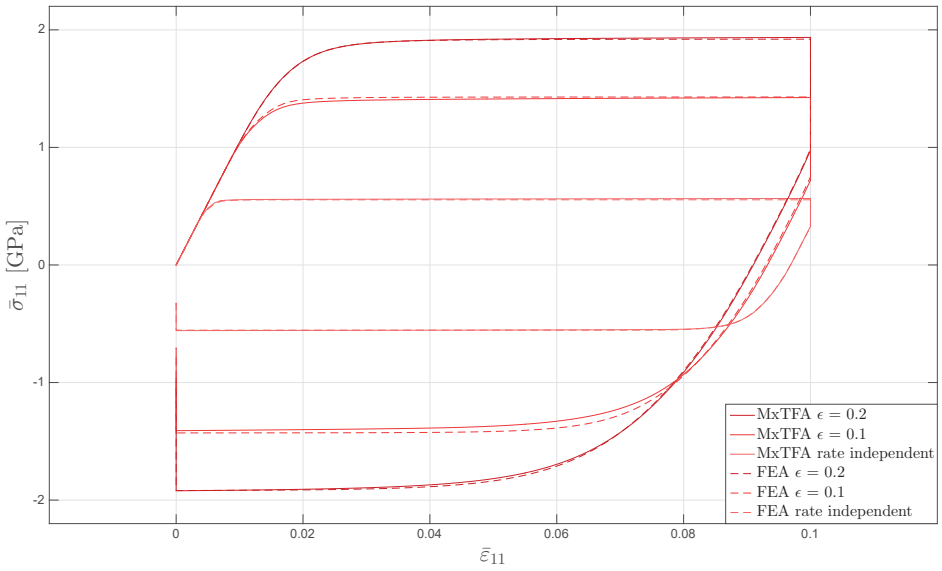

(a)

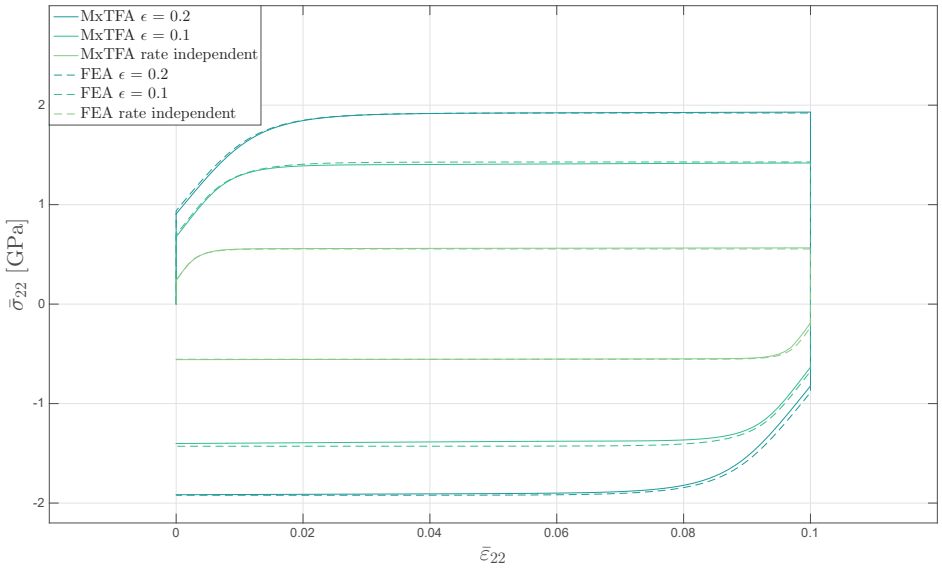

(b)

Figure 16: Test 2 - Mechanical response of the UC subjected to a bi-axial loading history: (a) mechanical response in x_1-direction; (b) mechanical response in x_2-direction.

of subsets characterized by the same computational burden. In particular, linear approximation is preferred with respect to the constant one. In fact, the use of a linear distribution leads to very satisfactory results.

The computational burden involved by the MxTFA is significantly lower than the FEA. In fact, at each time step the MxTFA procedure requires to solve the nonlinear system of equations (42) in order to determine the evolution of the history variables. On the contrary, the FEA requires to solve the evolution problem at the Gauss point level and the nonlinear equilibrium problem of the whole mesh. In particular, the MxTFA solves a system of nonlinear equations whose dimension is equal to the number of subsets times the 8 components of $\mathbf{U}^j$, while the FEA solves, at each Gauss point of each finite element, the nonlinear evolution problem consisting in 4 equations, 3 related to the inelastic strain components and 1 to the plastic multiplier.

Future developments will include on one side the extension of the MxTFA to other viscoplastic constitutive models in order to cover a wider range of problems, and on the other side the comparison of this technique with the proposal of [17], since it is also based on a mixed incremental variational form; other future works will also include the extension of this technique to 3D problems. In case of a 3D problem, it is expected that the number of internal variables and subsets will increase; however, the model can be successfully adopted to study 3D RVEs, as long as the composite is periodic. Keeping a linear distribution for stresses and a piecewise uniform distribution for the plastic multiplier the computational burden is still feasible. In addition, it should be noted that the pre-analyses are linear elastic and therefore are rather simple analyses to perform. For random composites (general microstructures) this procedure might become expensive from the computational point of view: for this reason, in this case some modifications in the approach of subset partitioning might be introduced, and this could be the subject of future developments.

On the basis of these considerations the MxTFA is an efficient tool to be adopted at the Gauss point level to determine the overall response of the composite material in the framework of multiscale analyses.

Acknowledgements

Financial supports by the Italian Ministry of Education, University and Research − MIUR are gratefully acknowledged:
PRIN2015 "Advanced mechanical modeling of new materials and structures for the solution of 2020 Horizon challenges" prot. 2015JW9NJT_018,
PRIN2015 "Multi-scale mechanical models for the design and optimization of micro-structured smart materials and metamaterials" prot. 2015LYYXA8_002.

References

[1] M.M. Aghdam and S.R. Morsali. Effects of manufacturing parameters on residual stresses in SiC/Ti composites by an elastic-viscoplastic micromechanical model. *Computational Materials Science*, 91:62 – 67, 2014.

[2] M. Agoras, R. Avazmohammadi, and P. Ponte-Castañeda. Incremental variational procedure for elasto-viscoplastic composites and application to polymer- and metal-matrix composites reinforced by spheroidal elastic particles. *International Journal of Solids and Structures*, 2016.

[3] A. Benedetti, S. de Miranda, and F. Ubertini. A posteriori error estimation based on the superconvergent recovery by compatibility in patches. *International Journal for Numerical Methods in Engineering*, 67:108–131, 2006.

[4] G. Castellazzi, S. de Miranda, and F. Ubertini. Patch based stress recovery for plate structures. *Computational Mechanics*, 47:379–394, 2011.

[5] J. Chaboche, L.S. Kruch, J. Maire, and T. Pottier. Towards a micromechanics based inelastic and damage modeling of composites. *International Journal of Plasticity*, 17:411–439, 2001.

[6] F. Covezzi, S. de Miranda, S. Marfia, and E. Sacco. Complementary formulation of the TFA for the elasto-plastic analysis of composites. *Composite Structures*, 2016.

[7] C. Czarnota, K. Kowalczyk-Gajewska, A. Salahouelhadj, M. Martiny, and S. Mercier. Modeling of the cyclic behavior of elastic-viscoplastic composites by the additive tangent Mori-Tanaka approach and validation by finite element calculations. *International Journal of Solids and Structures*, 56-57:96 – 117, 2015.

[8] F. Daghia, S. de Miranda, and F. Ubertini. Patch based recovery in finite element elastoplastic analysis. *Computational Mechanics*, 52:827–836, 2013.

[9] E.A. de Souza Neto, D. Perić, and D.R.J. Owen. *Computational Methods For Plasticity: Theory and Applications*. Wiley, 2008.

[10] G.J. Dvorak. Transformation field analysis of inelastic composite materials. *Proceedings of the Royal Society of London A*, 437:311–327, 1992.

[11] G.J. Dvorak and A. Bahei-El-Din. Inelastic composite materials: transformation field analysis and experiments. *In: Suquet, P. (Ed.), Continuum Micromechanics, CISM Course and Lecture*, 377:1–59, 1997.

[12] P. Franciosi and S. Berbenni. Heterogeneous crystal and poly-crystal plasticity modeling from transformation field analysis within a regularized schimd law. *Journal of Mechanics and Physics of Solids*, 55:2265–2299, 2007.

[13] P. Franciosi and S. Berbenni. Multi-laminate plastic-strain organization for nonuniform tfa modeling of poly-crystal regularized plastic flow. *International Journal of Plasticity*, 24:1549–1580, 2008.

[14] F. Fritzen and T. Böhlke. Three-dimensional finite element implementation of the nonuniform transformation field analysis. *International Journal for Numerical Methods in Engineering*, 278:186–217, 2010.

[15] F. Fritzen and T. Böhlke. Nonuniform transformation field analysis of materials with morphological anisotropy. *Composites Science and Technology*, 71:433–442, 2011.

[16] F. Fritzen, M. Hodapp, and M. Leuschner. GPU accelerated computational homogenization based on a variational approach in a reduced basis framework. *Computer Methods in Applied Mechanics and Engineering*, 278:186–217, 2014.

[17] F. Fritzen and M. Leuschner. Reduced basis hybrid computational homogenization based on a mixed incremental formulation. *Computer Methods in Applied Mechanics and Engineering*, 260:143–154, 2013.

[18] F. Fritzen, S. Marfia, and V. Sepe. Reduced order modeling in nonlinear homogenization: A comparative study. *Computers and Structures*, 157:114–131, 2015.

[19] R.M. Guedes, editor. *Creep and Fatigue in Polymer Matrix Composites*. Woodhead Publishing, 2011.

[20] T. Jiang, J.F. Shao, and W.Y. Xu. A micromechanical analysis of elastoplastic behavior of porous materials. *Mechanics Research Communications*, 38:437–442, 2011.

[21] N. Lahellec and P. Suquet. Effective response and field statistics in elasto-plastic and elasto-viscoplastic composites under radial and non-radial loadings. *International Journal of Plasticity*, 42:1 – 30, 2013.

[22] C. Mareau and S. Berbenni. An affine formulation for the self-consistent modeling of elasto-viscoplastic heterogeneous materials based on the translated field method. *International Journal of Plasticity*, 64:134 – 150, 2015.

[23] S. Marfia and E. Sacco. Multiscale damage contact-friction model for periodic masonry walls. *Computer Methods in Applied Mechanics and Engineering*, 205-208:189–203, 2012.

[24] S. Marfia and E. Sacco. Computational homogenization of composites experiencing plasticity, cracking and debonding phenomena. *Computer Methods in Applied Mechanics and Engineering*, 304:319 – 341, 2016.

[25] J.C. Michel and P. Suquet. Nonuniform transformation field analysis. *International Journal of Solids and Structures*, 40:6937–6955, 2003.

[26] J.C. Michel and P. Suquet. Computational analysis of nonlinear composite structures using the nonuniform transformation field analysis. *Computer Methods in Applied Mechanics and Engineering*, 193:5477–5502, 2004.

[27] D. Peric. On a class of constitutive equations in viscoplasticity: formulation and computational issues. *International Journal for Numerical Methods in Engineering*, 36:1365–1393, 1993.

[28] P. Perzyna. Fundamental problems in viscoplasticity. *Advances in Applied Mechanics*, 9(1):243 – 377, 1968.

[29] P. Ponte-Castañeda. New variational principles in plasticity and their application to composite materials. *Journal of the Mechanics and Physics of Solids*, 40(8):1757 – 1788, 1992.

[30] S. Roussette, J.C. Michel, and P. Suquet. Nonuniform transformation field analysis of elastic-viscoplastic composites. *Composites Science and Technology*, 69:22–27, 2009.

[31] E. Sacco. A nonlinear homogenization procedure for periodic masonry. *European Journal of Mechanics, A/Solids*, 28:209–222, 2009.

[32] V. Sepe, F. Auricchio, S. Marfia, and E. Sacco. Homogenization techniques for the analysis of porous sma. *Computational Mechanics*, 57(5):755–772, 2016.

[33] V. Sepe, S. Marfia, and E. Sacco. A nonuniform TFA homogenization technique based on piecewise interpolation functions of the inelastic field. *International Journal of Solids and Structures*, 50:725–742, 2013.

[34] D. Trias, J. Costa, J.A. Mayugo, and J.E. Hurtado. Random models versus periodic models for fibre reinforced composites. *Computational Materials Science*, 38(2):316–324, 2006.

[35] F. Ubertini. Patch recovery based on complementary energy. *International Journal for Numerical Methods in Engineering*, 59:1501–1538, 2004.